Transverse vibration of pre-stressed beams: An experimental technique for the determination of dynamic viscoelastic material properties of tissue mimicking materials

Yigit Yazicioglu[a], Bryn Martin[b], Karen Navarro-Castillo[c], Umit Kutluay[d] and Thomas Royston[c]

[a]Middle East Technical University, Orta Dogu Teknik Universitesi, Makine Muhendisligi Bolumu B-313, 06531 Ankara, Turkey
[b]University of Illinois at Chicago, 2923 W. 71st Street, Woodridge, IL 60517, USA
[c]University of Illinois at Chicago, 842 W. Taylor St. ERF 1072, Chicago, IL 60607, USA
[d]Tubitak-Sage, Samsun Yolu 25.Km, Tilkicak Tepe Mevkii P.K.16, 06261 Ankara, Turkey
yigit@metu.edu.tr

An experimental dynamic material property identification technique is presented that is based on the theoretical formulations of a vibrating pre-stressed beam. The technique determines the viscoelastic material properties of tissue mimicking materials that govern their dynamic behavior. Results are presented for a silicone based material (CF11-2188 Nusil Silicone Technology, Carpinteria, CA) that is in the form of a thick string held between fixed supports under tensile pre-stress. The specimens are excited through the transverse harmonic displacement of the boundary. Transverse vibration at an arbitrary location is measured and compared with theory to identify material viscoelastic moduli valid up to at least several hundred Hertz. The presented technique can aid in providing accurate viscoelastic parameter values for phantoms that are used in the development of a range of medical diagnostic techniques that attempt to identify pathology or tissue differentiation via changes in mechanical stiffness and viscosity.

1 Introduction

The quantification of the mechanical properties of various types of phantom materials has been of interest due to their use in constructing various types of compliant in vitro models of biological tissues. These compliant models have been used to test various types of novel sensor prototypes [1], mimic human anatomy of the cerebrospinal fluid system [2], lung cavity [3], brain [4], heart [5], vessels [6], and other complaint tissues. One robust quality of the in vitro studies is that they are often able to be used to perform measurements which are not possible in vivo. In addition, in vitro models remove the necessity for institutional review board approval on living subjects. However, for in vitro model results to be useful, it is critical that the material properties are quantified and made similar to in vivo. In general, the models have mimicked the in vivo elastic properties, but not done as well with mimicking the viscous damping provided by biological tissues. In addition, for the few in vitro studies which have detailed material properties, namely Young's modulus and Poisson's ratio [7], it was assumed that these properties are linear, while it is fairly well understood that silicone based materials exhibit frequency dependent material properties. Likewise, it is known that human tissue exhibits viscoelastic behavior [8], and this behavior changes substantially post mortem [9], compounding the challenge of accurately obtaining the mechanical properties of living tissue. Quantification of the viscoelastic properties of soft tissue-like materials has been performed by a number of researchers [10-15]. In the present study, we detail a technique for quantifying the viscoelastic properties of a compliant silicone based elastomer, which can be formed into a continuous thick beam. In particular, a silicone based elastomer, CF 11-2188, was chosen due to its low Young's modulus, which is similar in magnitude to that of human soft tissue. This material has been used to construct various compliant tissue and flow models [1, 3, 11, 16]. The proposed method of material property identification introduced here will lead to a set of parameters that are easy to use in theoretical calculations and computational studies.

2 Theory

The transverse vibration of the thick elastic phantom string can be modelled by using the governing equations of a vibrating string or pre-stressed thin beam. Due to the thickness of the specimen the effects of bending may not be negligible; therefore, a formulation that accounts for this is used.

The transverse motion of a pre-stressed elastic thin beam subject to excitation at its end is governed by the following equation [17],

$$\frac{\partial^4 y}{\partial x^4} - \frac{T}{EI}\frac{\partial^2 y}{\partial x^2} + \frac{1}{a^2}\frac{\partial^2 y}{\partial t^2} = 0 \qquad (1\text{-a})$$

where

$$a = \sqrt{\frac{EI}{\rho A}} . \qquad (1\text{-b})$$

Here, x is the longitudinal axis, y is the transverse displacement, E is the Young's Modulus, ρ is the material density, A is the beam cross sectional area, I is the moment of inertia of the cross section, and T is the axial force on the prestressed beam and is positive for tensile prestress.

If harmonic forcing is assumed as in the case of the experiment the normal mode harmonic solution can be taken as below:

$$y(x,t) = Y(x)e^{i\omega t} . \qquad (2)$$

The general solution for the above equation is given here directly.

$$Y(x) = A\cos(\alpha x) + B\sin(\alpha x) + C\cosh(\beta x) + D\sinh(\beta x). \qquad (3)$$

Here, the unknown coefficients A, B, C, and D depend on the boundary conditions and the wave numbers α and β are given as:

$$\alpha = \sqrt{-\varsigma + \sqrt{\varsigma^2 + \omega^2/a^2}} , \qquad (4\text{-a})$$

and

$$\beta = \sqrt{\varsigma + \sqrt{\varsigma^2 + \omega^2/a^2}} , \qquad (4\text{-b})$$

where,

$$\varsigma = \frac{T}{2EI} . \qquad (4\text{-c})$$

During the experiment, the pre-stressed beam is clamped at one end (no displacement or rotation) and driven with a harmonic displacement in the transverse y-direction from the support at the other end x = 0 m while constraining rotation at that end. (Fig. 1).

$$y(0,t) = Y_o e^{i\omega t} \qquad (5)$$

This will lead to the following boundary conditions:

$$\begin{aligned} Y(0) &= Y_o \\ Y'(0) &= 0 \\ Y(L) &= 0 \\ Y'(L) &= 0 \end{aligned} \qquad (6)$$
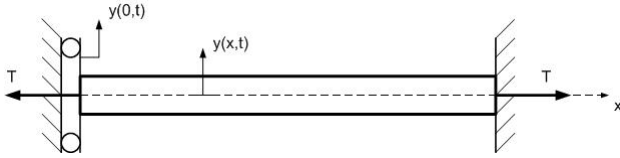
Fig. 1 The schematic of the pre-stressed fixed-fixed beam with transverse base excitation

The application of the boundary conditions to the given general solution results in the system of equations linear in terms of the unknown coefficients A, B, C, and D which can be solved algebraically by simple matrix inversion to yield:

$$A = \frac{\beta[\alpha[1 - \cos(\alpha L)\cosh(\beta L)] + \beta \sin(\alpha L)\sinh(\beta L)]}{2\alpha\beta[1 - \cos(\alpha L)\cosh(\beta L)] + (\beta^2 - \alpha^2)[\sin(\alpha L)\sinh(\beta L)]} Y_o$$

$$B = \frac{-\beta[\alpha \sin(\alpha L)\cosh(\beta L) + \beta \cos(\alpha L)\sinh(\beta L)]}{2\alpha\beta[1 - \cos(\alpha L)\cosh(\beta L)] + (\beta^2 - \alpha^2)[\sin(\alpha L)\sinh(\beta L)]} Y_o$$

$$C = \frac{-\alpha[\alpha \sin(\alpha L)\sinh(\beta L) + \beta[\cos(\alpha L)\cosh(\beta L) - 1]]}{2\alpha\beta[1 - \cos(\alpha L)\cosh(\beta L)] + (\beta^2 - \alpha^2)[\sin(\alpha L)\sinh(\beta L)]} Y_o$$

$$D = \frac{\alpha[\alpha \sin(\alpha L)\cosh(\beta L) + \beta \cos(\alpha L)\sinh(\beta L)]}{2\alpha\beta[1 - \cos(\alpha L)\cosh(\beta L)] + (\beta^2 - \alpha^2)[\sin(\alpha L)\sinh(\beta L)]} Y_o$$

$$(7)$$

3 Material model

The behavior of linear *viscoelastic* materials can be generally predicted using the Generalized Maxwell model [18]. The Generalized Maxwell model simulates the relaxations occurring at a distribution of times by the use of multiple numbers of spring and dashpot Maxwell elements arranged in parallel and series configuration as shown in Fig. 2. Some simple variations of the Generalized Maxwell model are the Maxwell model, Kelvin-Voigt model, and Standard Linear Solid (SLS) model.
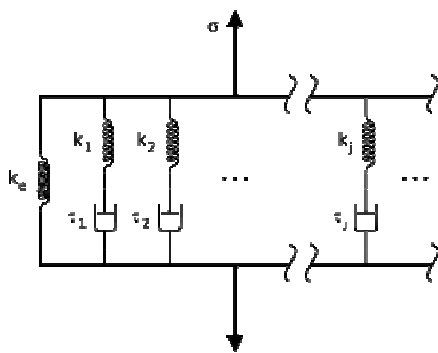

Fig. 2 Schematic of the Generalized Maxwell Model

Standard Linear Solid (SLS) model (Fig. 3) is used in this work for the formulations regarding the viscoelastic phantom material. The SLS model, also known as the Kelvin model [19], is a simplified version of Generalized Maxwell model where only first two arms (Hookean arm and the Maxwell arm) are kept. SLS model is considerably easier to use than the Generalized Maxwell model; it is more accurate than the Maxwell model in predicting creep, and it is superior to the Kelvin-Voigt model in predicting stress relaxation. [20]
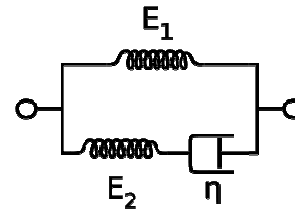

Fig. 3 Schematic of the Standard Linear Solid (SLS) Model

The differential relation between stress and strain for the SLS material shown in Fig. 3 is stated as follows:

$$\frac{d\sigma(t)}{dt} + \frac{E_2}{\eta}\sigma(t) = (E_1 + E_2)\frac{d\varepsilon(t)}{dt} + \frac{E_1 E_2}{\eta}\varepsilon(t). \quad (8)$$

Under harmonic excitation conditions this equation takes the following form:

$$\left[i\omega + \frac{E_2}{\eta}\right]\sigma(\omega) = \left[i\omega(E_1 + E_2) + \frac{E_1 E_2}{\eta}\right]\varepsilon(\omega). \quad (9)$$

The harmonic relation between the stress and strain can be written in the frequency domain as follows:

$$\sigma(\omega) = E^*(\omega) \cdot \varepsilon(\omega). \quad (10)$$

Here, E^* is the frequency dependent complex Young's modulus that also embodies viscoelastic properties and it can be shown it is in the following form:

$$E^*(\omega) = \frac{\dfrac{E_1 E_2}{\eta} + i\omega(E_1 + E_2)}{\dfrac{E_2}{\eta} + i\omega} \quad (11)$$

It can be observed that as E_2 stiffens the SLS model converges to Kelvin-Voigt model and as E_1 vanishes it acts as Maxwell model. (Fig. 4). It should also be noted that for static loading conditions and when frequency of excitation is low E^* simply becomes equal to E_1, the Young's modulus.
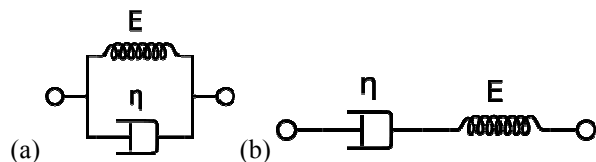

Fig. 4 Schematics of Kelvin-Voigt (a) and Maxwell (b) materials

4 Experimental work

An experimental setup is prepared to realize the problem formulated as given in the previous sections. The picture of the setup is shown in Fig. 5. The setup consists of two adjustable clamps that satisfy the fixed-fixed boundary conditions, one attached firmly to a fixed base and the other attached on an electromagnetic shaker (Bruel&Kjaer Type 4809 with Bruel&Kjaer Type 2706 Power Amplifier) for transverse excitation through the boundary at x = 0.

Silicon specimens were prepared by thoroughly mixing equal amounts of the two part CF11-2188 elastomer together for at least ten minutes. Note, the CF11-2188 elastomer is produced in large batches at the factory. The mechanical properties of the material vary from batch to batch, since the batch protocol at the factory is not

optimized to maintain consistent elastic properties of the cured material. For this reason, four separate batches of the material were obtained from the factory and tested, resulting in various material properties for each batch. The mixture was then degassed in a vacuum container (Nalgene 5305-0910, Rochester, NY) and then formed into thick strings by casting into large drinking straws. The specimens were then left to cure for one week at room temperature, after which they were carefully removed from the straws and cut to 10 cm unstressed lengths.

The cast specimens are mounted between the clamps and brought to the prescribed pretension (corresponding to 30% or 50% strain) that will lead to the tensile (positive) beam prestress. Retro-reflective tapes (3M) are attached to the top of the specimens and transverse vibration is measured at x = L/5 away from base excitation point using a laser doppler vibrometer (LDV)(Polytec CLV 800) together with the transverse boundary acceleration by means of an impedance head (PCB 288D01). A 0-400Hz broadband base excitation signal is provided by a dynamic signal analyzer (Agilent 35670A) which is used for the data acquisition purposes at the same time.
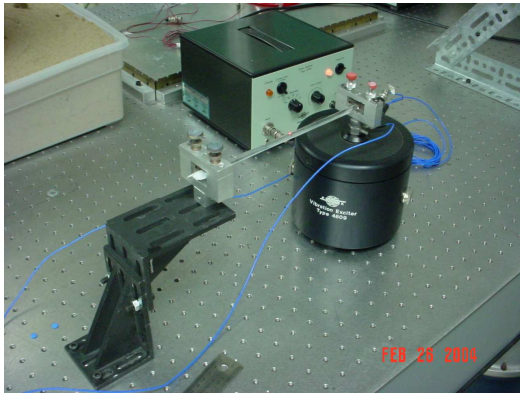

Fig. 5 Picture of the experiment setup for transverse vibration of pre-stressed silicon specimen

The data acquired from the experiment is the transfer function between the boundary acceleration and transverse beam velocity averaged 32 times. In order to obtain a normalized dimensional form this function is multiplied by an appropriate factor that also takes the sensor sensitivities into account, as shown in the following equation.

$$G(\omega) = \frac{\dot{Y}(x,\omega)\big|_{x=\frac{L}{5}}}{\ddot{Y}(x,\omega)\big|_{x=0}} \cdot i\omega \cdot k_{sensor} = \frac{\ddot{Y}(x,\omega)\big|_{x=\frac{L}{5}}}{\ddot{Y}(x,\omega)\big|_{x=0}} \cdot k_{sensor} = \frac{Y(x,\omega)\big|_{x=\frac{L}{5}}}{Y(x,\omega)\big|_{x=0}} \cdot k_{sensor}$$

(12)

5 Material property determination by hybrid optimization

Property determination involves finding an appropriate set of values for E_1, E_2, and η. Many approaches are possible. In this study, the set of material parameters are sought to obtain a match between the experimentally determined transfer function between the boundary excitation displacement and transverse vibration displacement $G(\omega|$ and the corresponding theoretical transfer function amplitude $Y(x)/Y_o$.

This becomes a three to one mapping type optimization problem with no constraints or lower/upper bounds. That is, the solution of an "unconstrained optimization problem", where the design parameters vector, X, is of length three and defined as:

$$X = \begin{bmatrix} E_1 & E_2 & \eta \end{bmatrix}^T \qquad (13)$$

Since, it is desired to find the "best" model that simulates data as close to the experimental data as possible, the objective (cost) function, which is to be minimized, should be selected as some kind of error function. Root Mean Square Error (RMSE) function is selected for this purpose, which can be expressed as:

$$P_E(x) = \left[\frac{1}{N} \cdot \sum_{j=1}^{N} \left(p_j(x) - \hat{p}_j(x) \right)^2 \right]^{\frac{1}{2}}$$

(14)

where p is the actual value and $\hat{p}$ is the estimated value of the function of x.

Experimental data is obtained as a complex function of frequency, i.e. for each frequency there is a magnitude and phase component (or the corresponding real and imaginary parts). Hence, there exist two RMSE functions, P_{RE} and P_{IMG}, one for the real parts and the other for the imaginary parts. In this way there exist not a single but two different objectives (multi-objective optimization):

1. Minimize the RMSE between the real parts of the experimental and the simulated data.
2. Minimize the RMSE between the imaginary parts of the experimental and the simulated data.

The method used, for the solution of this multi-objective optimization problem, is the weighted sum strategy, which converts the multi-objective optimization problem to a single objective problem by constructing a weighted sum of all of the objectives. As the result of the ongoing discussion, the objective function is selected as:

$$F_{obj}(X) =$$

$$w_1 \cdot \left[\frac{1}{N} \cdot \sum_{j=1}^{N} \left(\text{Re}\left(T_{Experiment_j}(X)\right) - \text{Re}\left(\hat{T}_{Simulation_j}(X)\right) \right)^2 \right]^{\frac{1}{2}} + w_2 \cdot \left[\frac{1}{N} \cdot \sum_{j=1}^{N} \left(\text{Im}\left(T_{Experiment_j}(X)\right) - \text{Im}\left(\hat{T}_{Simulation_j}(X)\right) \right)^2 \right]^{\frac{1}{2}}$$

(15)

where w_1 and w_2 are equally selected weights of 0.5 and N is the sample size.

The plots given in Fig. 6 show the behavior of objective function over a wide range of E_1, E_2, and η. As η increases, as seen from the figures, the objective function surface "smoothes" providing a global minimum valley. However, for smaller values of η, there exist many local extrema, hinting that a classical optimization method might fail to reach the global minimum. Therefore, a genetic algorithm is selected to be used for the solution of this problem. Genetic algorithms are mathematical methods for global search and optimization that are based on the mechanics of natural selection and science of genetics.

The mechanisms of biological and computational steps of genetic algorithm are explained in detail by Whorton [21]. Briefly summarizing his work, genetic algorithms consist of coding a population of candidate solutions and then operating on the population to determine the next generation. Iteration carries on for several generations until the population converges to a most fit solution. The next generation is determined by a mechanism of "natural selection", where the fitness of each member of the

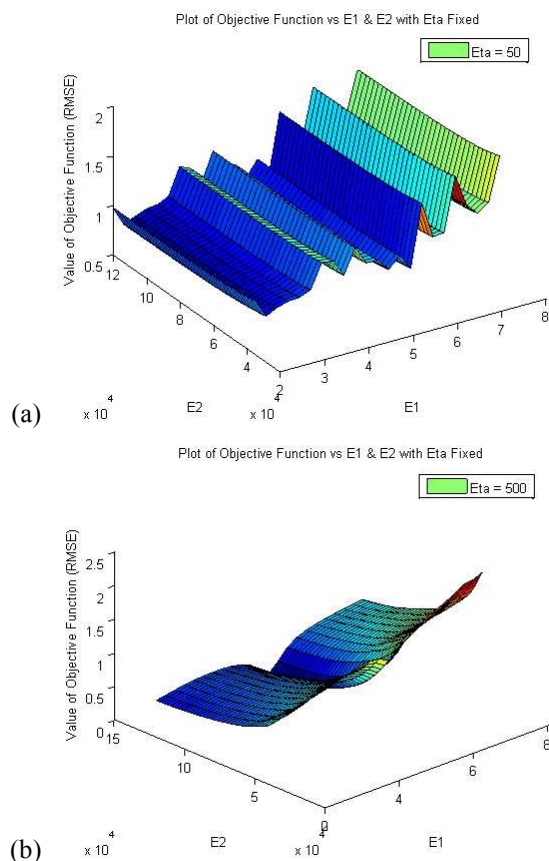population, based on the cost (objective) function is evaluated.

(a)

(b)

Fig. 6 Objective function behavior for
(a) η = 50 and (b) η = 500

Recently MathWorks (Natick, MA) have added the Genetic Algorithm and Direct Search Toolbox to their popular technical software package MATLAB™. In this study, their "ga" function from the above mentioned toolbox is utilized. The algorithm employed by the "ga" function of MATLAB™ can be summarized as follows where the algorithm:

1 Begins by creating a random initial population.

2 Creates a sequence of new populations. At each step, the algorithm uses the individuals in the current generation to create the next population following the steps:

a Computes the fitness value of each member of the current population.

b Selects members, called parents, based on their fitness.

c Some of the individuals in the current population that have lower fitness are chosen as *elite*. These elite individuals are passed directly to the next population.

d Produces children from the parents. Children are produced either by making random changes to a single parent—*mutation*—or by combining the vector entries of a pair of parents—*crossover*.

e Replaces the current population with the children to form the next generation.

3 Stops when one of the stopping criteria is met.
A well-known deficiency with the genetic algorithms is the time required to reach optimal solution. As a work around to this problem, a hybrid approach is utilized in this study, thus the genetic algorithm is run over a population of size 30 for 500 hundred generations. Although this relatively short run of genetic algorithm (computational time is about

10 minutes on a moderate PC) failed to reach the optimal solution, it provided a feasible starting point for classical gradient based optimization method (in this study, fminunc function of MATLAB™ is utilized for classical optimization) .

6   Results

The algorithm explained in previous section is run over the experimental data of four different batches of the same material, each batch having three different samples. Each sample is pre-strained to %30 and %50 percent of initial length. Thus, the algorithm was run for 24 cases.

Fig. 7 shows the response plots for experimental and simulated data for one of the cases (Batch 1, Sample 3 at 30% initial strain). As seen, the optimization algorithm gives quite acceptable accuracy over a range of several hundred Hz.
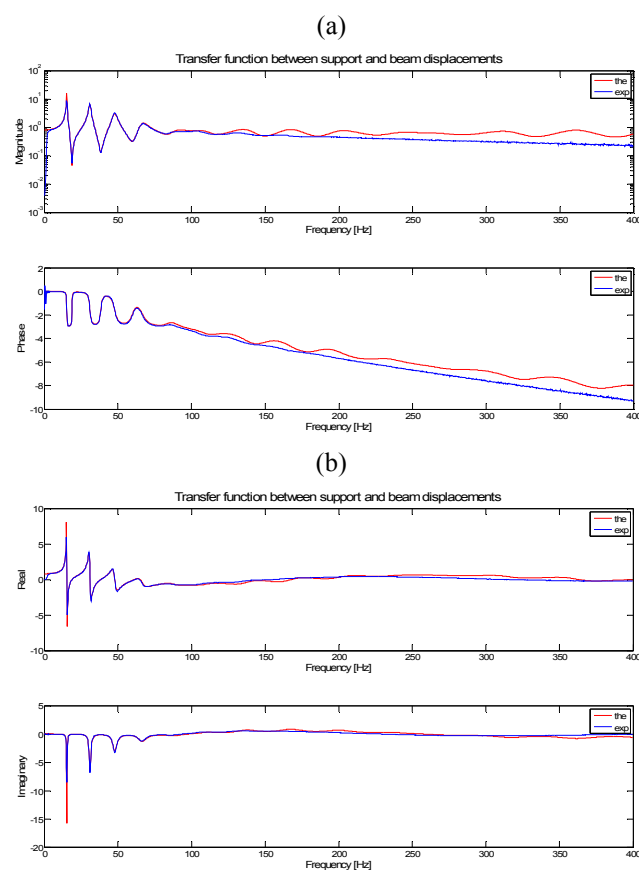
(a)

(b)

Fig. 7 Comparison of experimental and theoretical models
(a) Magnitude and phase vs. cyclic frequency (0-400Hz)
(b)Real and imaginary parts vs. cyclic frequency (0-400Hz)

To obtain the sample based parameters a weighted sum approach is utilized. For the same sample of material, data with different initial strains (30% and 50%) that gave minimum final objective function value was assigned the highest weight.

A similar weighted sum approach is utilized to obtain batch based parameters, but this time using all available information (all samples at all initial strain levels) for each batch of the material. Final results are provided in Table 1. Note that, for batches 2 and 4 the parameter search did not reach a solution for a finite E_2 so for those batches the search was done for E_1 and η, i.e. $E_2 = \infty$ for those batches.

Material	E_1 (Pa)	E_2 (Pa)	η (Pa·s)
B1	*55100.0*	*137344.9*	*317.0*
B2	*36520.4*	∞	*272.5*
B3	*155087.5*	*181803.6*	*306.3*
B4	*40367.6*	∞	*309.3*

Table 1 Estimated parameters for the different batches of the CF11-2188 material

7   Conclusion

A method was developed for the determination of viscoelastic material parameters of a silicone phantom material. The method uses data obtained from a simple vibration test which is compared with careful theoretical modeling of the experiment. The set of parameters that will result in the best match between the theory and experiment is sought by utilizing a hybrid optimization algorithm consisting of Genetic Algorithm and Unconstrained Optimization. It was observed that there were significant variations between different batches of the same material. These were in the form of numerical and behavioral variations where two batches (B1 & B3) acted as Standard Linear Solid, others (B2 & B4) acted as Kelvin-Voigt type.

Acknowledgments

References

[1]   T. Spohnholtz, T. J. Royston, Y. Yazicioglu, B. Martin, F. Loth, H. Bassiouny, "A multimode sonic and ultrasonic diagnostic imaging system with application to peripheral vascular characterization", *The Journal of the Acoustical Society of America,* v.117(4), p.2588, (2005).

[2]   W. Kalata, B. Martin, J. Oshinski, F. Loth, "Hydrodynamics of cerebrospinal fluid in spinal canal with chiari malformation and syringomyelia", *Proceedings of IMECE04 2004 ASME International Mechanical Engineering Congress*, p.1-2, (2004).

[3]   S. Acikgoz, M. B. Ozer, T. J. Royston, H. A. Mansy, R. H. Sandler, "Experimental and Computational Models for Simulating Sound Propagation Within the Lungs", *Journal of Vibration and Acoustics*, v.130(2), p.021010, (2008).

[4]   T. Seppälaa, J. Vähätalob, I. Auterinenc, A. Kosunend, D. W. Nigge, F. J. Wheelere and S. Savolainen, "Modelling of brain tissue substitutes for phantom materials in neutron capture therapy (NCT) dosimetry", *Radiation Physics and Chemistry*, v.55(3), p.239-246, (1999).

[5]   W. Sediono, O. Dössel, "Heart Phantom: A Simple Elastomechanical Model of Ventricle", *Proceedings CARS*, (2002).

[6]   R. D. Walker, R. E. Smith, S. B. Sherriff, and R F M Wood, "Latex vessels with customized compliance for use in arterial flow models", *Physiological. Measurement* v.20, p.277-286, (1999).

[7]   E. S. Drexler, A. J. Slifka, J. E. Wright, C. N. McCowan, D. S. Finch, T. P. Quinn, J. D. McColskey, D. D. Ivy, R. Shandas, "An Experimental Method for Measuring Mechanical Properties of Rat Pulmonary Arteries Verified With Latex", *Journal of Research of the National Institute of Standards and Technology*, v.108(3), p.183-191,(2003).

[8]   M. G. Dunn; F. H. Silver, "Viscoelastic Behavior of Human Connective Tissues: Relative Contribution of Viscous and Elastic Components", *Connective Tissue Research*, v.12(1), p. 59-70, (1983).

[9]   R. J. Oakland, R. M. Hall, R. K. Wilcox, D. C. Barton, "The Biomechanical Response of Spinal Cord Tissue to Uniaxial Loading", *Proceedings of the Institution of Mechanical Engineers, Part H: Journal of Engineering in Medicine*, v.220(4), p.489-492, (2006).

[10]   J. C. Conti, E. R. Strope, D. J. Rohde, L. D. Spence, "Frequency dependent radial compliance of latex tubing", Biomedical Sciences Instrumentation,v. 33, p.524-529, (1997).

[11]   H. A. Mansy, J. R. Grahe, R. H. Sandler, "Elastic properties of synthetic materials for soft tissuemodeling", Physics in Medicine and Biology, v.53, p.2115–2130, (2008).

[12]   E. F. Fabbroni, K. R. Shull, M. C. Hersam, "Adhesive and mechanical properties of soft nanocomposites: Model studies with blended latex films", *Journal of Polymer Science Part B: Polymer Physics*, v.39(24) , p.3090 – 3102, (2001).

[13]   J. Fromageau, E. Brusseau, D. Vray, G. Gimenez, P. Delachartre, "Characterization of PVA cryogel for intravascular ultrasound elasticity imaging", *IEEE Transactions on Ultrasonics, Ferroelectrics and Frequency Control*, v.50(10), p.1318-24, (2003).

[14]   C. Usha Devi and R. M. Vasu, A. K. Sood, "Design, fabrication, and characterization of a tissue-equivalent phantom for optical elastography", *Journal of Biomedical Optics* v.10(4), (2005).

[15]   W. F. Walker, F. J. Fernandez, L. A. Negron, "A method of imaging viscoelastic parameters with acoustic radiation force", Physics in Medicine and Biology v.45, p.1437–1447, (2000).

[16]   M. B. Ozer, S. Acikgoz, T. J. Royston, H. A. Mansy, R. H. Sandler, "Boundary element model for simulating sound propagation and source localization within the lungs", *The Journal of the Acoustical Society of America* v.122(1), p.657-671, (2007).

[17]   K. F. Graff, Wave Motion in Elastic Solids, Dover Publications, New York, (1991).

[18]   D. Roylance, Engineering Viscoelasticity, http://web.mit.edu/course/3/3.11/www/modules/visco.pdf, p.14-15, (2001).

[19]   Y. C. Fung, Biomechanics, p.41, Springer-Verlag, New York, (1993).

[20]   R. S. Lakes, Viscoelastic Solids, p.24-25, CRC Press, (1999).

[21]   M. S. Whorton, "Closed Loop System Identification with Genetic Algorithms", AIAA Paper, AIAA-2004-4887.